

# Matrix Element Effect in Layered PdSe<sub>2</sub>

Shimin Shan,<sup>†</sup> Fanxiang Meng,<sup>†</sup> Tongrui Li, Zhanfeng Liu, Yi Liu, Zhe Sun, Jingwei Dong,\*  
and Zhongwei Chen\*



Cite This: *J. Phys. Chem. C* 2025, 129, 4800–4805



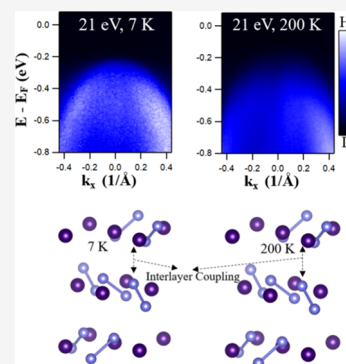
Read Online

ACCESS |

Metrics & More

Article Recommendations

**ABSTRACT:** Palladium diselenide (PdSe<sub>2</sub>), a novel two-dimensional dichalcogenide, has garnered widespread attention due to its exceptional optoelectronic properties. Unveiling the matrix element effect in layered semiconducting materials is essential for optimizing the performance of optoelectronic devices. However, no dedicated study has yet been reported on the photon energy and temperature dependence of this effect in PdSe<sub>2</sub>. In this work, we conducted a direct investigation of the electronic band structure of PdSe<sub>2</sub> as a function of temperature, employing photon-energy-dependent angle-resolved photoemission spectroscopy (ARPES). The wave vector asymmetry and signal drop at the valence band maximum stem from the matrix elements involved in the photoemission process. This effect is influenced by both the sample's temperature and the photon energy. Our findings provide clear, direct evidence of the matrix element effect in PdSe<sub>2</sub>, which is dependent on both the temperature and photon energy.



## INTRODUCTION

Due to their unique layer-dependent optical and dielectric properties, two-dimensional (2D) materials have demonstrated broad application prospects, emerging as essential components in the development of innovative optoelectronic devices.<sup>1–3</sup> Recently, a new class of 2D dichalcogenide materials (the formula is MX<sub>2</sub>, where M = Pd, Pt and X = S, Se) has garnered significant interest because of their distinct layer-dependent physical properties.<sup>4,5</sup> Among these, PdSe<sub>2</sub> features a unique puckered pentagonal structure, which endows it with significant potential for applications in optics, electronics, and thermoelectrics.<sup>6–10</sup> Furthermore, PdSe<sub>2</sub> not only exhibits excellent air stability, a unique linear dichroism conversion phenomenon, and high carrier mobility but also demonstrates long-wavelength infrared photoresponsivity and a wide adjustable bandgap that can be modified upon thickness, originating from the unusual interlayer couplings.<sup>6,11–13</sup> These properties make PdSe<sub>2</sub> an excellent candidate for the next generation of broadband polarization-sensitive photodetectors. For example, few-layered PdSe<sub>2</sub>, produced by mechanical exfoliation, has been currently utilized in the manufacture of photodetectors operating in the visible, infrared, and near-infrared spectra, demonstrating promising performance.<sup>9,12,14–16</sup>

A comprehensive understanding of the electronic band structure of PdSe<sub>2</sub> is crucial to improving its performance in practical applications. ARPES is a potent experimental technique for probing the electronic band structure and orbitals within crystals.<sup>17</sup> In ARPES measurements, photons are directed at a material, and the photoelectric effect is harnessed to determine the band structure. When the energy of the incident photons exceeds the energy required to liberate

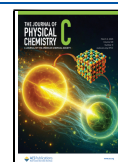
electrons from their bound states, electrons are emitted into the vacuum through the photoelectric effect. These emitted electrons are then captured by an electron analyzer, which measures their kinetic energy and emission angles. In a typical photoelectron spectroscopy experiment, the ARPES photoemission intensity  $I(\mathbf{k}, E)$  is proportional to the overlap integral between the initial state wave function  $\Psi_i$  and the final state wave function  $\Psi_f$ .  $I(\mathbf{k}, E)$  can be transformed according to the interaction operator  $H_{inv}$  to yield  $I(\mathbf{k}, E) \propto \sum_{f_i} |M_{f_i}^k|^2$ , where  $M_{f_i}^k$  is the photoemission matrix element ( $M_{f_i}^k = \Psi_f^k | \mathbf{A} \cdot \mathbf{P} | \Psi_i^k$ ,  $\mathbf{A}$  is the electromagnetic vector potential, and  $\mathbf{P}$  is the electronic momentum operator).  $M_{f_i}^k$  depends on the geometry of the experimental setup, the photon polarization, and the photon energy.<sup>18,19</sup> The matrix element does not directly reveal band dispersion; however, it can influence the intensity of photoemission signals. Specifically, the symmetry of the orbitals and their spatial distribution can cause certain matrix elements to vanish or peak for particular configurations, which, in turn, affects the observed band structure. Therefore, the matrix element effect is indispensable for gaining a deeper understanding of the physical properties of materials. For instance, polarization-dependent ARPES measurements reveal that the valence band top is primarily composed of Pd- $d_{3z^2-r^2}$

Received: January 2, 2025

Revised: February 13, 2025

Accepted: February 14, 2025

Published: February 20, 2025



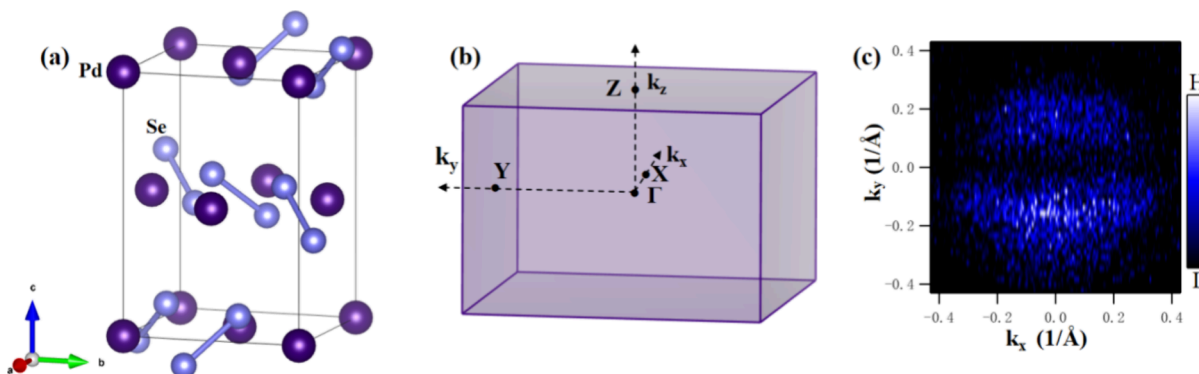


**Figure 1.** (a) Layered crystal structure of PdSe<sub>2</sub>. (b) Schematic diagram for the bulk Brillouin zone of PdSe<sub>2</sub>. (c) Constant-energy contour acquired at a binding energy of 0.4 eV by the p-polarized light ( $h\nu = 23$  eV).

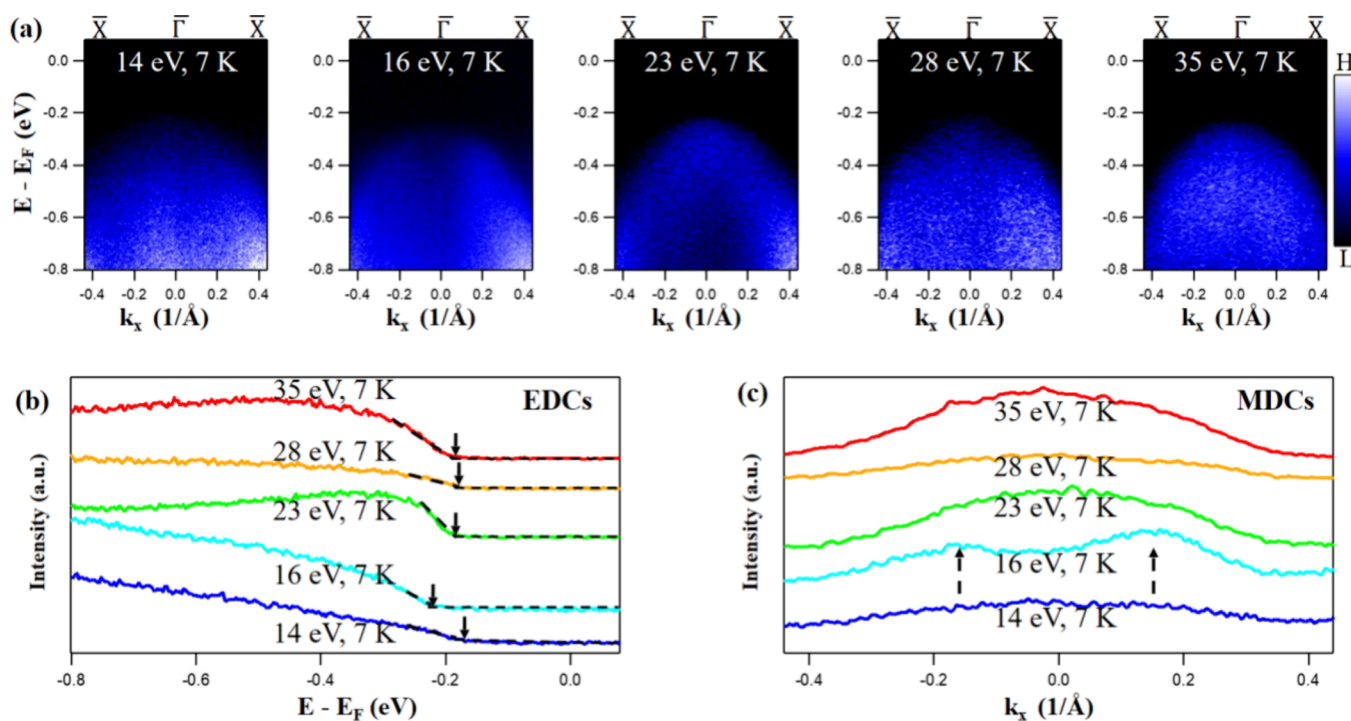


**Figure 2.** (a) High-resolution ARPES maps of PdSe<sub>2</sub> along the  $k_x$  high-symmetry direction in the photon energy range of 14–35 eV at 7 K. (b) Photon-energy-dependent energy distribution curve acquired at  $k_x = 0$  1/Å. The arrows represent the valence band tops. (c) Photon-energy-dependent momentum distribution curve acquired at  $E - E_F = -0.3$  eV. The arrows indicating the asymmetric band structure are marked in the panel.

and Se- $p_z$  orbitals.<sup>20</sup> Although the polarization-dependent matrix element effect in PdSe<sub>2</sub> has been examined, a comprehensive study exploring its correlation with photon energy and sample temperature has not been reported so far. Gaining a deeper understanding of these relationships can help bridge the gap between studies in the laboratory and practical applications of PdSe<sub>2</sub> at various photon energies and temperatures.

In this work, the roles of photon energy and sample temperature on the matrix element effect in PdSe<sub>2</sub> were investigated using photon-energy-dependent ARPES. By monitoring the valence band structures, we revealed that the wave vector asymmetry and signal drop at the valence band maximum, which are influenced by changes in photon energy and sample temperature, originate from the matrix elements involved in the photoemission process. This finding can primarily be attributed to the renormalization of interlayer

interactions. Our study not only illuminates the behaviors of the band structure in response to photon energy and temperature variations during the photoemission process but also lays the groundwork for versatile energy band engineering in the PdSe<sub>2</sub> semiconductor.

## EXPERIMENTAL DETAILS

The temperature-dependent ARPES data were acquired at the BL13U beamline of the National Synchrotron Radiation Laboratory (NSRL) in Hefei, China. The photon energy was tunable from 7 to 45 eV, ensuring the detection of electronic states from both the bulk and near-surface regions.<sup>21</sup> Extreme ultraviolet light shined onto the sample surface with an angle of 50°, and the beam spot size ( $H \times V$ ) at the sample position was about  $0.3 \times 0.3$  mm<sup>2</sup>. The light polarization was tuned by the horizontal movement of the elliptical polarization undulator (EPU), producing p/s-polarized (the electric field

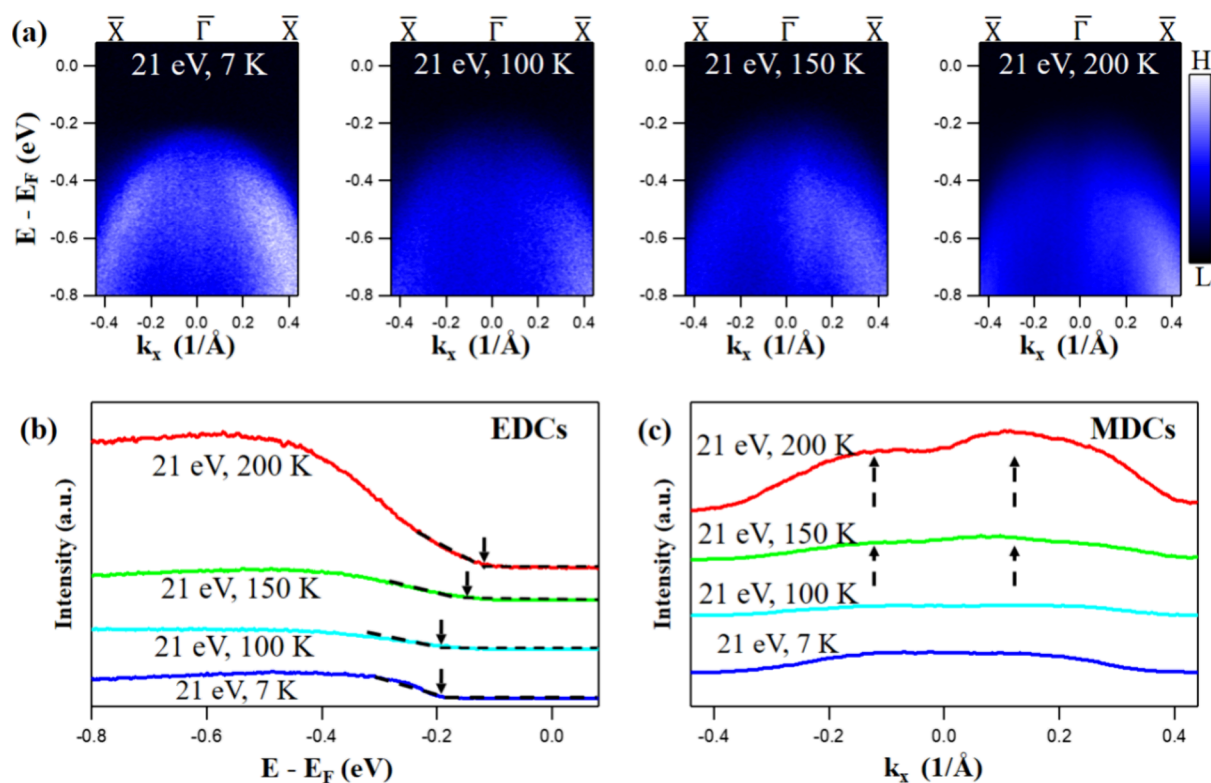


**Figure 3.** (a) ARPES maps along the  $k_x$  high-symmetry direction by the photon energy of 21 eV at various temperatures. (b) Temperature-dependent energy distribution curve acquired at  $k_x = 0$   $1/\text{\AA}$ . The arrows represent the valence band tops. (c) Temperature-dependent momentum distribution curve acquired at  $E - E_F = -0.3$  eV.

is parallel/vertical to the incident plane) beam. The photoelectrons were collected with a Scienta DA30 analyzer, equipped with an electrostatic lens, allowing Fermi surface mapping without sample rotation. The energy and momentum resolutions of the hemispherical analyzer were better than 15 meV and  $0.2^\circ$ , respectively. High-quality single crystals of PdSe<sub>2</sub> (thickness: 0.2 mm, lateral dimensions:  $1 \times 1$  mm<sup>2</sup>), purchased from Nanjing MKNANO Tech. Co., Ltd. ([www.mukenano.com](http://www.mukenano.com)), were cleaved at 7 K and measured under a base pressure of less than  $7 \times 10^{-11}$  Torr. The energy zero in all photoelectron spectra was set at the Fermi level that was referenced to a copper plate in electrical contact with the samples. No charging effect was observed during our measurements.

## RESULTS AND DISCUSSION

The crystal structure of the puckered layered PdSe<sub>2</sub> is shown in Figure 1a. A unit cell of PdSe<sub>2</sub> contains four Pd atoms and eight Se atoms, with two Se atoms crossing the Pd layer in the form of a Se–Se dumbbell. Layers interact via van der Waals forces, contributing to the material's stability. The bulk Brillouin zone of PdSe<sub>2</sub> (Figure 1b) is characterized by its high-symmetry directions, which are crucial for studying the electronic band structure. Key directions include  $k_x$ ,  $k_y$ , and  $k_z$ . These directions serve as pivotal references when examining the band structure, which reveals the semiconductor properties and the relationships between bands in PdSe<sub>2</sub>. The elliptical pockets in the constant-energy contour at a binding energy of 0.4 eV by a p-polarized light of 23 eV, as shown in Figure 1c, allow us to identify the two high-symmetry directions  $k_x$  and  $k_y$ . Moreover, the signal drop at  $k_x = \pm 0.2$  ( $1/\text{\AA}$ ) and  $k_y = 0$  ( $1/\text{\AA}$ ) is due to the polarization-dependent matrix element

effect.<sup>20</sup> This effect has been observed in another puckered layered semiconductor of black phosphorus.<sup>22</sup>

The ARPES maps of PdSe<sub>2</sub> along the  $k_x$  high-symmetry direction acquired at 7 K by various photon energies are shown in Figure 2a. Normally, ultraviolet (UV) beams primarily provide photoemission maps from the bulk (photon energy of 14 eV) to the near-surface region (photon energy of 35 eV) of samples, which is determined by the inelastic mean free path (IMFP) of the emitted photoelectrons.<sup>21</sup> In layered materials such as PdSe<sub>2</sub>, the sample depth probed by ARPES depends on the inelastic mean free path of the emitted photoelectrons, which is a function of the photon energy used in the experiment. In terms of PdSe<sub>2</sub>, the IMFP varies with photon energy, allowing ARPES to probe electronic states from the near-surface region (shallow depth) to the bulk region (deeper depth). This variation in sample depth is particularly significant in PdSe<sub>2</sub> due to its puckered layered structure, where the strength of interlayer interactions changes with depth. When ARPES probes different depths within the sample, the strength of interlayer interactions varies due to the changing local environment. For example, at shallow depths (near-surface region), the interlayer interactions are weaker because the surface layer experiences reduced coordination with neighboring layers. At greater depths (bulk region), the interlayer interactions are stronger due to the increased coordination and overlap of orbitals between adjacent layers. This variation in interlayer interaction strength with depth is reflected in the ARPES intensity maps. This leads to observable changes in the valence band structure, such as shifts in the valence band maximum (VBM) and variations in the photoemission intensity. The varying sample depth in the puckered 2D PdSe<sub>2</sub> corresponds to differing strengths of interlayer

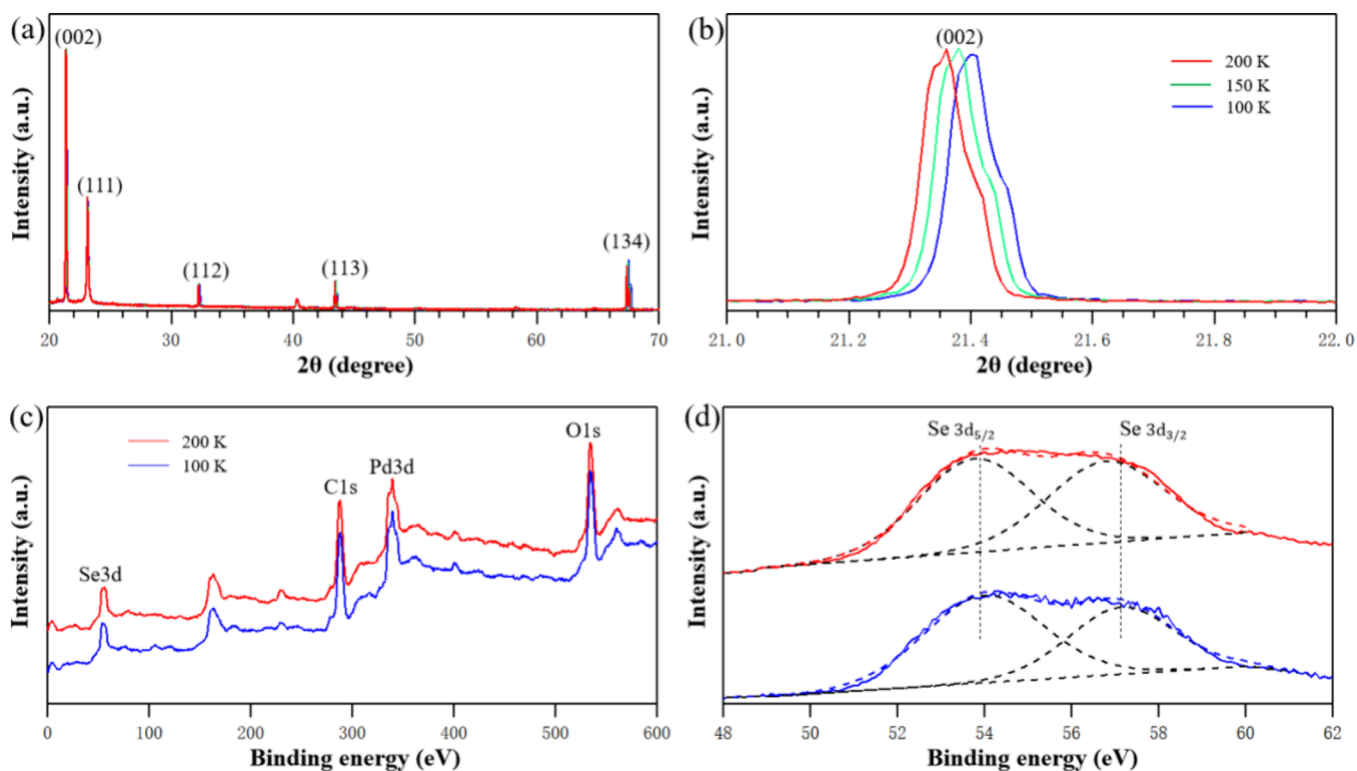


**Figure 4.** (a) Powder XRD patterns of PdSe<sub>2</sub> as a function of the temperature. The crystal planes are labeled in the figure. (b) Shift of the (002) peak toward the smaller angle upon heating. (c, d) High-resolution XPS of the PdSe<sub>2</sub> crystal obtained at 200 and 100 K. Green curves and cyan curves (d) represent the Se3d<sub>5/2</sub> and Se3d<sub>3/2</sub> fit results at 200 and 100 K, respectively.

interactions.<sup>23</sup> Similarly, puckered black phosphorus exhibits an evident interlayer interaction evolution as a function of sample thickness.<sup>24</sup> According to a previous report,<sup>23</sup> the VBM top has an out-of-plane character (Pd- $d_{3z^2-r^2}$ ), and the strong interlayer bonding along the *c*-axis can be ascribed to the strong directional character of Pd and Se dimers. The puckered structure of PdSe<sub>2</sub> further enhances this effect, as the out-of-plane Pd-*d* and Se-*p* orbitals play significant roles in determining the interlayer coupling. The hybridization of these orbitals changes with depth, leading to a renormalization of the electronic band structure as a function of sample depth. This renormalization is particularly evident in the wave vector asymmetry and signal drop observed in the ARPES data, which are directly influenced by the matrix element effects arising from the varying interlayer interactions.

The interlayer interactions in PdSe<sub>2</sub> are influenced by the puckered geometry of the layers. In PdSe<sub>2</sub>, the interlayer Se–Se distance (3.75 Å) is significantly larger than the intralayer Se–Se distance (2.36 Å), leading to relatively weak interlayer coupling compared to other transition-metal dichalcogenides (TMDs) like PtSe<sub>2</sub> (3.27 Å) or CrSe<sub>2</sub> (3.59 Å).<sup>25,26</sup> However, the directionality of the Pd-*d* and Se-*p* orbitals still contributes to non-negligible interlayer interactions, particularly along the *c*-axis. A more pronounced wave vector asymmetry and signal drop at the valence band maximum are observed at a photon energy of 16 eV (Figure 2a). This suggests that it is possible to selectively enhance the emission from bonding states in PdSe<sub>2</sub> by adjusting the photon energy. Additionally, the ARPES maps obtained with different photon energies exhibit varying photoelectron intensity structures. The photon-energy-dependent ARPES maps confirm that the matrix element effect in PdSe<sub>2</sub> is influenced by the injected photon energy. This is

attributed to the varying impact of different interlayer interaction strengths on the bonding states of Pd- $d_{3z^2-r^2}$  and Se-*p<sub>z</sub>* orbitals.<sup>27</sup> To quantitatively analyze matrix elemental effects in Figure 2a, we plot energy distribution curves (EDCs) acquired at  $k_x = 0$  1/Å and momentum distribution curves (MDCs) acquired at  $E - E_F = -0.3$  eV in Figure 2b,c, respectively. As shown in Figure 2b, the top of the valence band using 16 eV exhibits a significant shift toward higher binding energies when using 16 eV, compared to other energy scenarios. Similarly, in Figure 2c, the arrows indicate a distinctly asymmetric band structure that occurs also at 16 eV.

Temperature often serves as an effective parameter for adjusting the band gaps of semiconductors.<sup>28–30</sup> As the temperature increases, the thermal expansion of the lattice can lead to changes in the interlayer distance. The expansion of the lattice can affect the electronic structure and bonding interactions within the material. The temperature-dependent interlayer coupling has been certified in black phosphorus.<sup>31</sup> The primary role in the temperature-dependent bandgap renormalization is played by the contribution of interlayer interactions. Figure 3a shows the ARPES maps acquired at 7, 100, 150, and 200 K by 21 eV. The top of the valence band exhibits a clear change upon heating; specifically, the wave vector asymmetry and signal drop become more pronounced as the temperature increases. The EDCs acquired at  $k_x = 0$  1/Å and MDCs acquired at  $E - E_F = -0.3$  eV are shown in Figure 3b,c, respectively. Due to the Fermi–Dirac distribution of electrons upon heating, the matrix element effect cannot be observed by the valence band top shift in Figure 3b. Fortunately, as shown by the arrows in Figure 3c, the wave vector asymmetry and the signal drop become more pronounced with increasing temperature. This finding should

be attributed to the influence of interlayer coupling renormalization on the orbital hybridization of the bonding states upon heating. In the context of Pd-*d* and Se-*p* orbitals, the change in interlayer distance due to thermal expansion can influence the hybridization between these orbitals. The hybridization between metal *d*-orbitals and chalcogen *p*-orbitals (such as Pd-*d* and Se-*p*) is crucial for determining the electronic properties of PdSe<sub>2</sub>. Theoretical studies have shown that the electronic structure and bonding interactions in such materials are sensitive to the interatomic distances.<sup>32</sup> When the interlayer distance changes due to thermal expansion, the overlap between the Pd-*d* and Se-*p* orbitals is altered, which can affect the hybridization state.

Specifically, an increase in the interlayer distance can lead to a reduction in the overlap between the orbitals, potentially weakening the hybridization. This temperature effect can result in changes to the electronic band structure and density of states, which in turn can influence the material's properties such as electrical conductivity and thermal conductivity.<sup>33</sup> Therefore, the thermal expansion of the lattice and the resulting changes in interlayer distance can significantly impact the hybridization of Pd-*d* and Se-*p* orbitals, affecting the overall electronic and thermal properties of the material. The change of hybridization of Pd-*d* and Se-*p* orbitals in PdSe<sub>2</sub> due to the interlayer coupling renormalization upon heating can lead to the matrix element effect of the wave vector asymmetry and signal drop when the other experimental parameters remain stable.

Normally, temperature variation may lead to changes of defect density.<sup>34</sup> In order to clarify the role of defects in the band top evolution upon heating, X-ray diffraction (XRD) and X-ray photoelectron spectroscopy (XPS) measurements have been employed. Figure 4a,b illustrates the normal peak shift upon heating, with no appearance or disappearance of new peaks with temperature changes. Selenium vacancies are commonly detected as the primary defect in PdSe<sub>2</sub> crystals.<sup>35</sup> In terms of our measurements, the Se 3*d*<sub>3/2</sub> and Se 3*d*<sub>5/2</sub> orbitals exhibit a negligible shift upon heating, as shown in Figure 4d. Therefore, we propose that electron-defect scattering remains consistent across the entire temperature range in our study, without introducing additional wave vector asymmetry or signal drop.

## CONCLUSIONS

In conclusion, the valence band structure of PdSe<sub>2</sub> was measured at different temperatures using photon-energy-dependent ARPES. We observed that the wave vector asymmetry and signal drop at the valence band maximum in the photoemission process are dependent on both photon energy and sample temperature. This finding can primarily be attributed to the renormalization of interlayer interactions, which are influenced by sample depth and temperature. Our study lays the groundwork for bridging the gap between laboratory research and the practical deployment of layered PdSe<sub>2</sub>, facilitating the transition from theoretical insights to real-world applications.

## AUTHOR INFORMATION

### Corresponding Authors

**Jingwei Dong** – Power Battery and Systems Research Center and State Key Laboratory of Catalysis, Dalian Institute of Chemical Physics, Chinese Academy of Sciences, Dalian 116023, China; Email: [djw1991@dicp.ac.cn](mailto:djw1991@dicp.ac.cn)

**Zhongwei Chen** – Power Battery and Systems Research Center and State Key Laboratory of Catalysis, Dalian Institute of Chemical Physics, Chinese Academy of Sciences, Dalian 116023, China; [orcid.org/0000-0003-3463-5509](https://orcid.org/0000-0003-3463-5509); Email: [zwchen@dicp.ac.cn](mailto:zwchen@dicp.ac.cn)

### Authors

**Shimin Shan** – School of Semiconductors and Physics, North University of China, Taiyuan 030051, China; [orcid.org/0009-0007-8521-7549](https://orcid.org/0009-0007-8521-7549)

**Fanxiang Meng** – Power Battery and Systems Research Center and State Key Laboratory of Catalysis, Dalian Institute of Chemical Physics, Chinese Academy of Sciences, Dalian 116023, China

**Tongrui Li** – National Synchrotron Radiation Laboratory, University of Science and Technology of China, Hefei 230029, China; [orcid.org/0009-0002-4214-2018](https://orcid.org/0009-0002-4214-2018)

**Zhanfeng Liu** – National Synchrotron Radiation Laboratory, University of Science and Technology of China, Hefei 230029, China

**Yi Liu** – National Synchrotron Radiation Laboratory, University of Science and Technology of China, Hefei 230029, China

**Zhe Sun** – National Synchrotron Radiation Laboratory, University of Science and Technology of China, Hefei 230029, China

Complete contact information is available at:

<https://pubs.acs.org/10.1021/acs.jpcc.5c00015>

### Author Contributions

<sup>†</sup>S.S. and F.M. contributed equally to this work.

### Notes

The authors declare no competing financial interest.

## ACKNOWLEDGMENTS

This work is supported by the Natural Science Foundation of China (Grant No. 22409194), the Energy Revolution S&T Program of Yulin Innovation Institute of Clean Energy, (Grant No. YICE E411060316), the Strategic Priority Research Program of the Chinese Academy of Sciences (Grant No. XDB0600000, XDB0600200), the Fundamental Research Program of Shanxi Province (Grant No. 202203021212116), and the Natural Science Foundation of Liaoning Province (Grant No. 2024BSBA27).

## REFERENCES

- (1) Chhowalla, M.; Shin, H. S.; Eda, G.; Li, L.-J.; Loh, K. P.; Zhang, H. The chemistry of two-dimensional layered transition metal dichalcogenide nanosheets. *Nat. Chem.* **2013**, *5* (4), 263–275.
- (2) Zhang, E.; Jin, Y.; Yuan, X.; Wang, W.; Zhang, C.; Tang, L.; Liu, S.; Zhou, P.; Hu, W.; Xiu, F. ReS<sub>2</sub>-based field-effect transistors and photodetectors. *Adv. Funct. Mater.* **2015**, *25* (26), 4076–4082.
- (3) Li, N.; Zhang, Y.; Cheng, R.; Wang, J.; Li, J.; Wang, Z.; Sendeku, M. G.; Huang, W.; Yao, Y.; Wen, Y.; et al. Synthesis and optoelectronic applications of a stable p-type 2D material:  $\alpha$ -MnS. *ACS Nano* **2019**, *13* (11), 12662–12670.
- (4) Pi, L.; Li, L.; Liu, K.; Zhang, Q.; Li, H.; Zhai, T. Recent Progress on 2D Noble-Transition-Metal Dichalcogenides. *Adv. Funct. Mater.* **2019**, *29* (51), No. 1904932.
- (5) Kempt, R.; Kuc, A.; Heine, T. Two-Dimensional Noble-Metal Chalcogenides and Phosphochalcogenides. *Angew. Chem., Int. Ed.* **2020**, *59* (24), 9242–9254.
- (6) Soulard, C.; Rocquefelte, X.; Petit, P. E.; Evain, M.; Jobic, S.; Itié, J. P.; Munsch, P.; Koo, H. J.; Whangbo, M. H. Experimental and

- theoretical investigation on the relative stability of the PdSe<sub>2</sub>- and Pyrite-type structures of PdSe<sub>2</sub>. *Inorg. Chem.* **2004**, *43* (6), 1943–1949.
- (7) Oyedele, A. D.; Yang, S.; Liang, L.; Puztzky, A. A.; Wang, K.; Zheng, J.; Yu, P.; Pudasaini, P. R.; Ghosh, A. W.; Liu, Z.; et al. PdSe<sub>2</sub>: pentagonal two-dimensional layers with high air stability for electronics. *J. Am. Chem. Soc.* **2017**, *139* (40), 14090–14097.
- (8) Sun, J.; Shi, H.; Siegrist, T.; Singh, D. J. Electronic, transport, and optical properties of bulk and mono-layer PdSe<sub>2</sub>. *Appl. Phys. Lett.* **2015**, *107* (15), 153902.
- (9) Liang, Q.; Wang, Q.; Zhang, Q.; Wei, J.; Lim, S. X.; Zhu, R.; Hu, J.; Wei, W.; Lee, C.; Sow, C.; et al. High-Performance, Room Temperature, Ultra-Broadband Photodetectors Based on Air-Stable PdSe<sub>2</sub>. *Adv. Mater.* **2019**, *31* (24), No. 1807609.
- (10) Qin, D.; Yan, P.; Ding, G.; Ge, X.; Song, H.; Gao, G. Monolayer PdSe<sub>2</sub>: a promising two-dimensional thermoelectric material. *Sci. Rep.* **2018**, *8*, 2764.
- (11) Chow, W. L.; Yu, P.; Liu, F.; Hong, J.; Wang, X.; Zeng, Q.; Hsu, C.-H.; Zhu, C.; Zhou, J.; Wang, X.; et al. High mobility 2D palladium diselenide field-effect transistors with tunable ambipolar characteristics. *Adv. Mater.* **2017**, *29* (21), No. 1602969.
- (12) Long, M.; Wang, Y.; Wang, P.; Zhou, X.; Xia, H.; Luo, C.; Huang, S.; Zhang, G.; Yan, H.; Fan, Z.; et al. Palladium Diselenide Long-Wavelength Infrared Photodetector with High Sensitivity and Stability. *ACS Nano* **2019**, *13* (2), 2511–2519.
- (13) Yu, J.; Kuang, X.; Gao, Y.; Wang, Y.; Chen, K.; Ding, Z.; Liu, J.; Cong, C.; He, J.; Liu, Z.; et al. Direct observation of the linear dichroism transition in two dimensional palladium diselenide. *Nano Lett.* **2020**, *20* (2), 1172–1182.
- (14) Zeng, L.-H.; Wu, D.; Lin, S.-H.; Xie, C.; Yuan, H.-Y.; Lu, W.; Lau, S. P.; Chai, Y.; Luo, L.-B.; Li, Z.-J.; et al. Controlled Synthesis of 2D Palladium Diselenide for Sensitive Photodetector Applications. *Adv. Funct. Mater.* **2019**, *29* (1), No. 1806878.
- (15) Luo, L.-B.; Wang, D.; Xie, C.; Hu, J.-G.; Zhao, X.-Y.; Liang, F.-X. PdSe<sub>2</sub> multilayer on germanium nanocones array with light trapping effect for sensitive infrared photodetector and image sensing application. *Adv. Funct. Mater.* **2019**, *29* (22), No. 1900849.
- (16) Zhong, J.; Yu, J.; Cao, L.; Zeng, C.; Ding, J.; Cong, C.; Liu, Z.; Liu, Y. High-performance polarization-sensitive photodetector based on a few-layered PdSe<sub>2</sub> nanosheet. *Nano Res.* **2020**, *13* (6), 1780–1786.
- (17) Lv, B.; Qian, T.; Ding, H. Angle-resolved photoemission spectroscopy and its application to topological materials. *Nat. Rev. Phys.* **2019**, *1* (10), 609–626.
- (18) Shen, Z. X. Angle-resolved photoemission spectroscopy studies of cuprate superconductors. *Front. Sci.* **2002**, *75*, 71–94.
- (19) Sobota, J. A.; He, Y.; Shen, Z.-X. Angle-resolved photoemission studies of quantum materials. *Rev. Mod. Phys.* **2021**, *93* (2), No. 025006.
- (20) Gu, C.; Liu, X.; Chen, C.; Liang, A.; Guo, W.; Yang, X.; Zhou, J.; Jozwiak, C.; Bostwick, A.; Liu, Z.; et al. Low-lying electronic states with giant linear dichroism ratio observed in PdSe<sub>2</sub>. *Phys. Rev. B* **2022**, *106* (12), No. L121110.
- (21) Seah, M. P.; Dench, W. A. Quantitative electron spectroscopy of surfaces: A standard data base for electron inelastic mean free paths in solids. *Surf. Interface Anal.* **1979**, *1* (1), 2–11.
- (22) Jung, S. W.; Ryu, S. H.; Shin, W. J.; Sohn, Y.; Huh, M.; Koch, R. J.; Jozwiak, C.; Rotenberg, E.; Bostwick, A.; Kim, K. S. Black phosphorus as a bipolar pseudospin semiconductor. *Nat. Mater.* **2020**, *19* (3), 277–281.
- (23) Ryu, J. H.; Kim, J.-G.; Kim, B.; Kim, K.; Kim, S.; Park, J.-H.; Park, B.-G.; Kim, Y.; Ko, K.-T.; Lee, K. Direct observation of orbital driven strong interlayer coupling in puckered two-dimensional PdSe<sub>2</sub>. *Small* **2022**, *18* (9), No. 2106053.
- (24) Margot, F.; Lisi, S.; Cucchi, I.; Cappelli, E.; Hunter, A.; Gutierrez-Lezama, I.; Ma, K.; von Rohr, F.; Berthod, C.; Petocchi, F.; et al. Electronic Structure of Few-Layer Black Phosphorus from  $\mu$ -ARPES. *Nano Lett.* **2023**, *23* (14), 6433–6439.
- (25) Vanbruggen, C. F.; Haange, R. J.; Wieggers, G. A.; Deboer, D. K. G. CrSe<sub>2</sub>, a new layered dichalcogenide. *Physica B & C* **1980**, *99* (1–4), 166–172.
- (26) Zhao, Y.; Qiao, J.; Yu, Z.; Yu, P.; Xu, K.; Lau, S. P.; Zhou, W.; Liu, Z.; Wang, X.; Ji, W.; et al. High-electron-mobility and air-stable 2D layered PtSe<sub>2</sub> FETs. *Adv. Mater.* **2017**, *29* (5), No. 1604230.
- (27) Cattelan, M.; Sayers, C. J.; Wolverson, D.; Carpena, E. Site-specific symmetry sensitivity of angle-resolved photoemission spectroscopy in layered palladium diselenide. *2D Mater.* **2021**, *8*, No. 045036.
- (28) Fan, H. Y. Temperature dependence of the energy gap in semiconductors. *Physica* **1951**, *82* (6), 900–905.
- (29) Cardona, M.; Meyer, T. A.; Thewalt, M. L. W. Temperature dependence of the energy gap of semiconductors in the low-temperature limit. *Phys. Rev. Lett.* **2004**, *92* (19), No. 196403.
- (30) Chen, C.; Chen, F.; Chen, X.; Deng, B.; Eng, B.; Jung, D.; Guo, Q.; Yuan, S.; Watanabe, K.; Taniguchi, T.; et al. Bright mid-infrared photoluminescence from thin-film black phosphorus. *Nano Lett.* **2019**, *19* (3), 1488–1493.
- (31) Huang, S.; Wang, F.; Zhang, G.; Song, C.; Lei, Y.; Xing, Q.; Wang, C.; Zhang, Y.; Zhang, J.; Xie, Y.; et al. From anomalous to normal: temperature dependence of the band gap in two-dimensional black phosphorus. *Phys. Rev. Lett.* **2020**, *125* (15), No. 156802.
- (32) Huang, Z. Q.; Xu, J. Q.; Huang, H. H. Theoretical analysis of the thermoelectric properties of penta-PdX<sub>2</sub> (X = Se, Te) monolayer. *Front. Chem.* **2022**, *10*, No. 1061703.
- (33) Tong, Y. F.; Bouaziz, M.; Oughaddou, H.; Enriquez, H.; Chaouchi, K.; Nicolas, F.; Kubsy, F.; Esaulov, V.; Bendounan, A. Phase transition and thermal stability of epitaxial PtSe<sub>2</sub> nanolayer on Pt (111). *RSC Adv.* **2020**, *10*, 30934.
- (34) Li, J. V.; Levi, D. H. Determining the defect density of states by temperature derivative admittance spectroscopy. *J. Appl. Phys.* **2011**, *109* (8), No. 083701.
- (35) Jena, T.; Hossain, M. T.; Nath, U.; Sarma, M.; Sugimoto, H.; Fujii, M.; Giri, P. K. Evidence for intrinsic defects and nanopores as hotspots in 2D PdSe<sub>2</sub> dendrites for plasmon-free SERS substrate with a high enhancement factor. *npj 2D Mater. Appl.* **2023**, *7* (1), 8.